Unambiguous determination of local orientations of polycrystalline $CuInSe_2$ thin films via dictionary-based indexing

M. De Graef[1], W.C. Lenthe[1], N. Schäfer[2], T. Rissom[2], D. Abou-Ras[2]

[1] Department of Materials Science and Engineering, Carnegie Mellon University, Pittsburgh, PA 15213, USA
[2] Helmholtz-Zentrum Berlin für Materialien und Energie GmbH, Hahn-Meitner-Platz 1, 14109 Berlin, Germany

Abstract
The present work describes the approach of how to determine local orientations in individual $CuInSe_2$ grains from electron-backscatter diffraction (EBSD) data, in spite of the very small deviation (0.3%) of the ratio of lattice constants of the tetragonal crystal structure, *c*/*a*, from the value in the pseudocubic case, 2. A dictionary-based indexing algorithm is applied on each EBSD pattern, determining unambiguously the corresponding $CuInSe_2$ crystal orientation of the tetragonal structure. The approach provided in the present work can be used to improve the studies of microstructure-property relationships in various relevant photovoltaic material systems with similar pseudosymmetrical crystal structures, such as kesterite-type or halide-perovskite thin films.

Thin-film solar cells based on polycrystalline $Cu(In,Ga)Se_2$ have reached conversion efficiencies of around 23% in the recent years [1]. As an important part of the research and development of these photovoltaic devices, (micro)structure-property relationships have been investigated by various research groups (e.g., [2]). One issue linked to these relationships is the correct determination of local crystal orientations of the tetragonal $Cu(In,Ga)Se_2$ crystals. This determination is complicated by the ratio of the lattice constant of the tetragonal structure, c/a, which is very close to 2 for all compounds in the $Cu(In,Ga)Se_2$ solid solution. When changing the concentration ratio x=[Ga]/([Ga]+[In]) (GGI) in this solid solution from 0 to 100%, i.e., from the ternary $CuInSe_2$ to the ternary $CuGaSe_2$, the tetragonal distortion ($c/2a$ - 1) varies linearly from about 0.3% to about -2% [3].
As already outlined and studied by Kiely et al. [4] as well as by Casey et al. [5], this distortion may affect the stacking of the atomic lattice during the $Cu(In,Ga)Se_2$ thin-film growth, resulting in domain or inversion boundaries, since different variants (orientations of unit cells which would be symmetrically equivalent in a cubic structure but are not in the tetragonal structure) may coexist. The influence of such domains on the electrical properties of the $Cu(In,Ga)Se_2$ thin film has not yet been studied in detail. An appropriate strategy would be to identify these domains via electron backscatter diffraction (EBSD) and then to correlate this information with other scanning electron and probe microscopy techniques on the identical positions.
For polycrystalline $CuGaSe_2$ thin films, it was possible to reveal the tetragonal distortion ($c/2a$ - 1 = -2%) in EBSD maps, whereas for polycrystalline $CuInSe_2$, the applied algorithm failed [6]. Also in general, local orientations of crystals with a tetragonal distortion of $c/2a$ - 1<1-2% have not yet been correctly identified (see, e.g., Ref. 7 and references therein).

In the present work, we demonstrate the successful application of dictionary indexing of EBSD patterns on maps acquired on polycrystalline $CuInSe_2$ thin films. We describe the used algorithm and show how it can be applied to determine unambiguously the local orientations of individual $CuInSe_2$ crystal orientations.

2. Experimental details

The investigated $CuInSe_2$ thin films were produced by three-stage co-evaporation [8] on Mo-coated glass substrates. The HR-EBSD measurements were conducted using a Zeiss Ultraplus SEM equipped with an Oxford Instruments NordlysNano camera. Best EBSD pattern quality was achieved using an accelerating voltage of 15 kV, high beam current of up to 55 nA and 1x1 binning.

3. Dictionary Indexing of EBSD Patterns

The Hough-based pattern indexing algorithm available in the vendor analysis software is not able to distinguish between the *a*- and *c*-axis orientations for the $CuInSe_2$ phase. The recently developed Dictionary Indexing technique [9] uses a physics-based model to accurately predict EBSD patterns for a given crystal structure, microscope accelerating voltage, detector geometry and grain orientation. The model is based on an EBSD master pattern, i.e., a stereographic projection of the back-scattered electron yield on the Kikuchi sphere. For 15 kV electrons, the yield is shown in Fig. 1(a) for the $CuInSe_2$ structure; the crystallographic *c*-axis is normal to the projection, and the *a*-axis points horizontally towards the right. The pattern in (b) shows the absolute difference between the reference pattern in (a) and a similar pattern rotated 90° around the crystallographic *a*-axis, i.e., the pseudo-symmetrically equivalent orientation. The maximum intensity in (b) is about 20% of the maximum intensity in (a), indicating that the differences between the two pseudo-symmetrically related orientations are not very large. The highest intensities in (b) occur near the <110] zone axes, indicating that the traditional indexing based on the Hough transform may be able to index patterns that contain <110]-type zone axes; the similarity between the two patterns is highest for the <100] and [001] zone axis orientations.

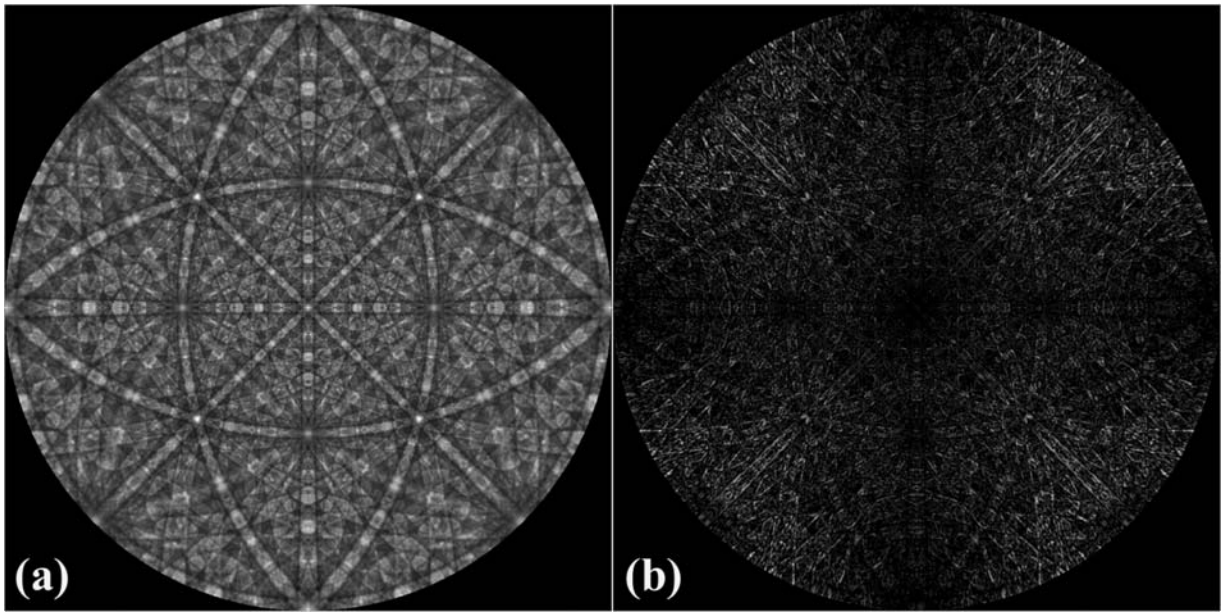

Figure 1: (a) 15 kV EBSD master pattern (stereographic projection with c-axis normal to map, and a-axis pointing to the right); (b) difference map between the map in (a) and a similar map rotated by 90° around the *a*-axis. The maximum intensity in (b) is 20% of the maximum in (a).

The most critical aspect of orientation determination in the presence of pseudo-symmetry is the accurate determination of the detector parameters, i.e., the pattern center coordinates (x^*,y^*) and the sample-scintillator distance z^*. For the $CuInSe_2$ data set, a grain with a prominent [221] zone axis near the center of the pattern provides the best orientation to refine the detector parameters. Fig. 2(b) shows an average dot product map for the complete data set; the intensity in each pixel is proportional to the average dot product of the corresponding EBSD pattern with the patterns of the four nearest neighbors. The grain in the upper left corner produces the EBSD pattern in Fig. 2(a) after averaging of all patterns inside the white square of 11x11 pixels. A refinement algorithm was used to determine both the grain orientation and the detector parameters; two different similarity metrics were used for the refinement, namely the dot product between experimental and simulated patterns, and the mutual information [10]. Once the orientation was determined, two additional orientations were tested by interchanging the crystallographic *c* axis with the *a* and *b* axes; this corresponds to rotating the crystal structure by 120° and 240° around the [221] pole in Fig. 2(a). The dot product values for the correct orientation and the two rotated orientations are [0.96207, 0.96155, 0.96165]; the mutual information values are [0.156466, 0.150957, 0.149474]. In each case the first value is the higher one, indicating a higher pattern similarity. The refined detector parameters for the first case were then used to index the complete data set; the resulting parameters are (x^*,y^*,z^*) = (0.4990,0.5231,0.4965), and the refined orientation is (23.93°, 71.66°,100.74°) in Bunge Euler angles.

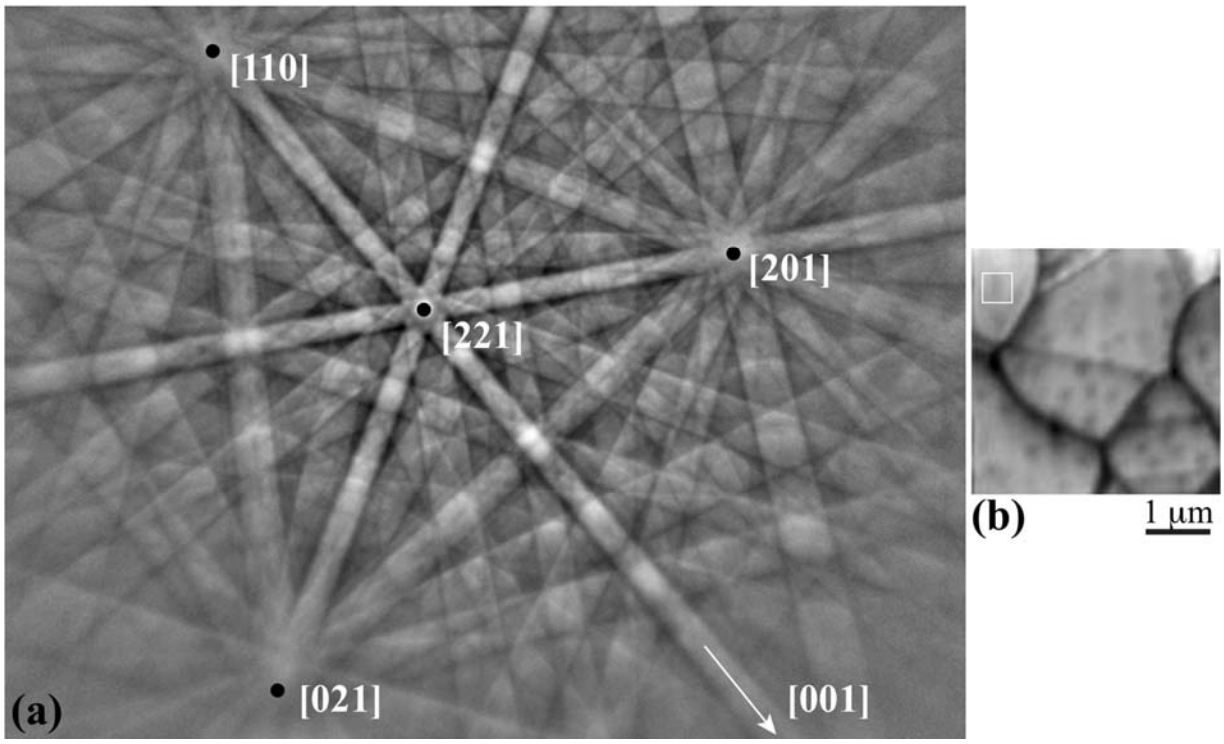

Figure 2: (a) Averaged EBSD pattern over the square region in (b); the intensities in (b) correspond to the average dot product of an EBSD pattern with the patterns of the four nearest neighbor acquisition points.

A pattern dictionary is generated by simulating patterns for the refined geometrical detector parameters as well as a uniform sampling of orientation space [11]. Each experimental pattern is compared to all dictionary patterns using a similarity metric, in this case the normalized dot product between the patterns. The grain orientation of the dictionary pattern that has the highest similarity to a given experimental pattern is then assigned as the orientation of the experimental pattern. This approach has been shown to be robust against noise [12], and is capable of distinguishing between patterns that are very similar [13].

Once the pattern orientations have been determined, an orientation refinement step can be applied in which the orientation is allowed to freely change to maximize the similarity between the experimental and simulated patterns. The refinement is carried out for two different starting orientations, namely the original orientation determined by the dictionary indexing algorithm and the pseudo-symmetrically equivalent orientation determined by rotating the original orientation by 90°@[010]; the final orientation corresponds to the highest dot product for the two simulated patterns.

4. Results and discussion

Figure 3 shows on the top row (a-c) the EBSD orientation distribution maps according to the [100], [010], and [001] inverse pole figures (IPFs) based on the Hough indexing approach. Some of the grains and several grain boundaries are rather noisy, an indication that the indexing algorithm was not able to decide on the actual orientation. The middle row (d-f) shows the equivalent EBSD orientation distribution maps based on the dictionary indexing results. Note that, with the exception of the grain labelled 3 in (a), the maps are less noisy. More importantly, the grain colors are different from the colors in the top row for most grains; only the grains labelled 1 and 2 in (a) have the same color. The map in Fig. 3h shows the disorientation between the Hough results and the dictionary results as a grayscale image with intensity range from 0° (black) to 90° (white); grains 1 and 2 are dark in this map, indicating that the orientations are very similar in both indexing approaches. For all other grains, the disorientation is around 90°, indicating that they are misindexed in the Hough approach due to pseudosymmetry. The map in Fig. 3g shows the EBSD pattern quality using the “pattern sharpness” parameter defined in Ref. 14; it is interesting that the grains with the highest pattern sharpness also correspond to the ones that are consistently indexed for both indexing approaches.

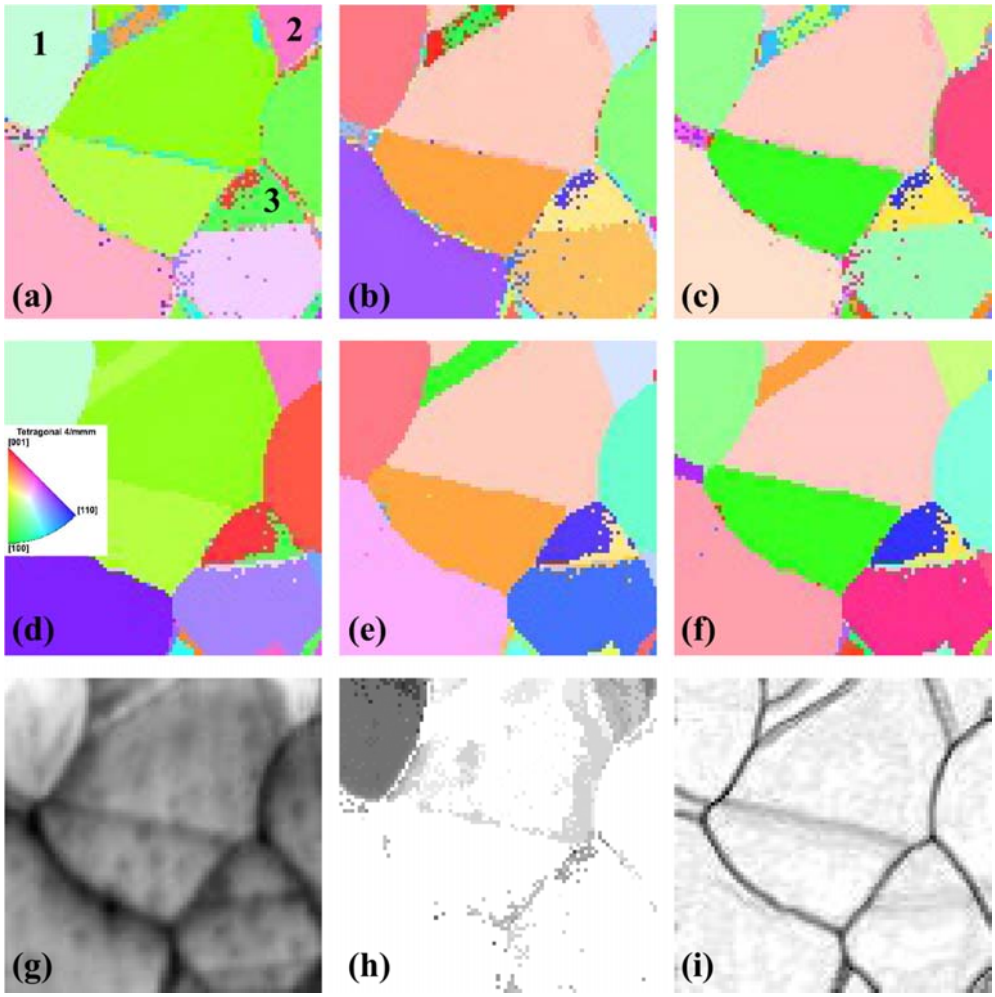

Figure 3: (a)-(c) Hough indexing results (orientation-distribution maps) displayed as [100], [010], and [001] inverse pole figures (IPFs); (d)-(f) IPFs from dictionary indexing after orientation refinement; (g) pattern quality map; (h) disorientation map between Hough and dictionary indexing results (black=0°, white = 90°); orientation similarity map using the top 20 dictionary indexing results.

Finally, the map given in Fig. 3i is the orientation similarity map (OSM). The dictionary indexing approach ranks the dot products between each experimental pattern and the entire set of dictionary patterns; the OSM then shows how many of the top *N* matches each pixel has in common, on average, with its four nearest neighbors (for this analysis, *N* was set to 20). The grain boundaries are clearly delineated since they correspond to sampling locations for which the lists of top near matches are different. Note also that several of the boundaries have a fuzzy appearance; this is likely owing to the fact that the grain boundary has a shallow inclination angle with respect to the sample surface.
We note that the orientation-distribution maps in Figs. 3d-f do not indicate the presence of the domain boundaries mentioned above (see Refs. 4 and 5) within individual grains, with the exception of grain no. 3, which exhibits two domains with a misorientation of 90° around [100]. In a future research effort, such domains will be further investigated in high-efficient $CuInSe_2$ and $Cu(In,Ga)Se_2$ thin films, in order to reveal their electrical and optoelectronic properties.

5. Conclusions

In the present work, we demonstrated the successful application of the dictionary indexing approach to EBSD patterns recorded from a polycrystalline $CuInSe_2$ thin film exhibiting a pseudocubic (tetragonal) crystal structure, in which the ratio of the lattice constants *c*/*a* exhibits a very small deviation from 2 of only 0.3%. Thus, it is possible to determine unambiguously local orientations of grains and to identify crystallographic features such as inversion/domain boundaries within individual grains. The approach provided in the present work can be used to improve the studies of microstructure-property relationships in various relevant photovoltaic material systems apart from $Cu(In,Ga)Se_2$ with similar pseudosymmetrical crystal structures, such as kesterite-type or halide-perovskite thin films.

Acknowledgements

N.S. and D.A. are grateful for financial support by the Helmholtz Virtual Institute “Microstructure Control for Thin-Film Solar Cells” (VH-VI-520) and by the BMWi project EFFCIS (No. 0324076B). M.D.G. and W.C.L. acknowledge financial support from an ONR/Vannevar Bush Faculty Fellowship program # N00014-16-1-2821 and grant MCF-677785 for use of the computational resources of the Materials Characterization Facility at Carnegie Mellon University.

References

[1] P. Jackson, R. Wuerz, D. Hariskos, E. Lotter, W. Witte, M. Powalla, *Phys. Stat. Solidi (RRL)* **2016**, *10*, 583.
[2] D. Abou-Ras, S.S. Schmidt, N. Schäfer, J. Kavalakkatt, T. Rissom, T. Unold, R. Mainz, A. Weber, T. Kirchartz, E. Simsek Sanli, P.A. van Aken, Q.M. Ramasse, H.-J. Kleebe, D. Azulay, I. Balberg, O. Millo, O. Cojocaru-Mirédin, D. Barragan-Yani, K. Albe, J. Haarstrich, C. Ronning, *Phys. Stat. Sol. (RRL)* **2016**, *10*, 363.
[3] D. Abou-Ras R. Caballero C. A. Kaufmann M. Nichterwitz K. Sakurai S. Schorr T. Unold H. W. Schock, *Phys. Stat. Sol. (RRL)* **2008**, *2*, 135.
[4] C.J. Kiely, R.C. Pond, G. Kenshole, A. Rockett, *Phil. Mag. A* **1991**, *63*, 1249
[5] S.M. Casey, C.A. Mullan, C.J. Kiely, R.C. Pond, R.D. Tomlinson, *Inst. Phys. Conf. Ser.* **1991**, *117*, 379.
[6] D. Abou-Ras, J. Gibmeier, G. Nolze, A. Gholinia, P. Konijnenberg, *Cryst. Res. Techn.* **2008**, *43*, 234.
[7] B. Jackson, D. Fullwood, J. Christensen, S. Wright, *J. Appl. Cryst.* **2018**, *51*, 655.
[8] C. A. Kaufmann, R. Caballero, T. Unold, R. Hesse, R. Klenk, S. Schorr, M. Nichterwitz, H.-W. Schock, *Sol. En. Mater. Sol. Cells* **2009**, *93*, 859.
[9] Y.H. Chen, S.U. Park, D. Wei, G. Newstadt, M.A. Jackson, J.P. Simmons, M. De Graef, A.O. Hero, *Microsc. Microanal.* **2015**, *21*, 739.
[10] E.B. Gulsoy, J.P. Simmons, M. De Graef, *Scripta Mater.* **2009**, *60*, 381.
[11] S. Singh, M. De Graef, *Modelling Simul. Mater. Sci. Eng.* **2016**, *24*, 085013.
[12] S.I. Wright, M.M. Nowell, S.P. Lindeman, P.P. Camus, M. De Graef, M.A. Jackson, *Ultramicroscopy*, **2015**, *159*, 81.
[13] M.J. Burch, C.M. Fancher, S. Patala, E.C. Dickey, and M. De Graef, *Ultramicroscopy* **2017**, *173*, 47.
[14] N.C. Krieger Lassen, Automatic Determination of Crystal Orientation from Electron Backscattering Patterns, Ph.D. thesis, The Technical University of Denmark, 1994.